Journal of Industrial and Engineering Chemistry xxx (2019) xxx–xxx

Contents lists available at ScienceDirect

Journal of Industrial and Engineering Chemistry

journal homepage: www.elsevier.com/locate/jiec

Exploration of a novel Type II 1D-ZnO nanorods/$BiVO_4$ heterojunction photocatalyst for water depollution

Jang Sen Chang[a], Yi Wen Phuan[b,c], Meng Nan Chong[a,*], Joey D. Ocon[d]

[a] School of Engineering, Chemical Engineering Discipline, Monash University Malaysia, Jalan Lagoon Selatan, Bandar Sunway, Selangor DE 47500, Malaysia
[b] School of Energy and Chemical Engineering, Xiamen University Malaysia, Selangor DE 43900, Malaysia
[c] College of Chemistry and Chemical Engineering, Xiamen University, Xiamen 361005, China
[d] Laboratory of Electrochemical Engineering (LEE), Department of Chemical Engineering, University of the Philippines Diliman, Quezon City 1101, Philippines

ARTICLE INFO

Article history:
Received 2 October 2019
Received in revised form 14 November 2019
Accepted 2 December 2019
Available online xxx

Keywords:
1D-ZnO nanorods
Bismuth vanadate ($BiVO_4$)
Heterojunction photocatalysts
Photocatalytic degradation
Type II heterojunction

ABSTRACT

In this study, we reported on the successful fabrication of a novel heterojunction photocatalyst (in particulate system) with a Type II band alignment between 1D-ZnO nanorods and $BiVO_4$ nanocrystals. Pristine 1D-ZnO nanorods and $BiVO_4$ nanocrystals were first fabricated through hydrothermal reaction followed by heterojunction formation via the wet chemical reaction. The 1D-ZnO/x$BiVO_4$ heterojunction photocatalyst (x = weight ratio of $BiVO_4$ in g) that found optimum when x = 0.08 g was used for the degradation of salicylic acid (SA) and Reactive Black 5 (RB5) resulting in high pseudo-first-order reaction rate constants of 0.0049 min^{-1} and 0.0132 min^{-1}, respectively. Electrochemical studies proved that the 1D-ZnO/0.08$BiVO_4$ heterojunction photocatalyst demonstrated a fast charge mobility and the most efficient photogenerated charge carriers separation among other heterojunction samples as analysed from PL spectra. Besides, UV–vis spectroscopic measurement and optical characterisation showed that the improved photoactivity in 1D-ZnO/$BiVO_4$ is attributed to the formation of a Type II heterojunction staggered arrangement that enables a broader visible-light harvesting ability. Finally, a postulation photocatalytic mechanism was proposed based on the theoretical band alignment diagram between the 1D-ZnO nanorods and $BiVO_4$ nanocrystals as well as portraying the fundamental charge carriers transfer within the 1D-ZnO/$BiVO_4$ heterojunction photocatalyst.

Introduction

The application of advanced oxidation processes (AOPs) for water depollution is widely-documented for its capacity in decomposing a wide variety of recalcitrant organics into readily biodegradable compounds, innocuous carbon dioxide and water molecules [1–9]. Among the AOPs, semiconductor-based photocatalysis is a direct and green water depollution process for rapid and complete mineralisation of organic pollutants via in situ production of active oxidative species, such as superoxide anion radicals ($^{\bullet}O_2^-$), hydroxyl radicals ($^{\bullet}OH$), and photogenerated holes (h^+) [10–14]. In this regard, zinc oxide (ZnO) is a semiconductor-based photocatalyst that has been widely exploited due to its low cost, non-toxicity nature, high chemical stability, and excellent photo-responsiveness [15,16]. Additionally, the semiconductor ZnO metal oxide is a highly versatile photocatalyst that could be synthesized into various controlled physical structures and morphologies with distinct physicochemical properties, such as ZnO nanoparticles [17,18], ZnO nanorods [19,20], ZnO nanowires [21,22], ZnO nanosheets [23,24], and ZnO nanoflowers [25,26]. Among the various physical structures and morphologies of ZnO, the one-dimensional (1D) ZnO nanorod has received considerable scientific interests due to its high proportion of active polar surfaces, unidirectional charge transport, fast charge carrier mobility, high electron trapping efficiency and electron delocalisation [27,28].

Nevertheless, the application of 1D-ZnO as a visible-light driven photocatalyst has been a practical challenge as it possesses a wide band gap energy (E_g) of 3.37 eV that confines its absorption in solar spectrum to the light radiation wavelength shorter than 400 nm. This means that the 1D-ZnO photocatalyst can only be excited by ultraviolet (UV) light, which accounts for 3–5% of the total solar spectrum to drive the overall photocatalytic reaction [29]. In order to retain the distinct physicochemical properties of 1D-ZnO while also broadening its visible spectral response (i.e. 44–47% of the total solar spectrum), several modifications have been pursued, including elemental doping of metals and non-metals [30–33], surface deposition with noble metals [34,35], and coupling with

* Corresponding author.
E-mail address: Chong.Meng.Nan@monash.edu (M.N. Chong).

https://doi.org/10.1016/j.jiec.2019.12.002
1226-086X/

other semiconductors [36,37]. To date, there are a number of studies that coupled ZnO with other semiconductors leading to the formation of heterojunction structures with appropriate band alignments [36,38–40]. The formation of heterojunction structure in ZnO is able to broaden its visible-light harvesting, promote fast charge mobility, enable efficient separation of photogenerated charge carriers and thus, enhancing the overall photocatalytic performance [41,42].

Theoretically, a heterojunction structure requires an effective pairing between a low-to-mid-energy band gap semiconductor (i.e. acts as light absorber) and high-energy band gap semiconductors that straddle in terms of the position of their valence and conduction bands [43]. In this regard, the mid-energy band gap semiconductor bismuth vanadate ($BiVO_4$) of 2.4 eV is considered as a suitable candidate for heterojunction pairing with ZnO of 3.2 eV as the former could act as an effective light absorber into the visible spectrum for improving the overall photocatalytic efficiency [44–46]. The unique band structure of highly-ordered $BiVO_4$ consisting of V 3d orbitals for conduction band and Bi 6s, O 2p hybrid orbitals for valence band has made $BiVO_4$ to be promising for application in photocatalytic water depollution. Whilst $BiVO_4$ possesses numerous distinct physicochemical properties, $BiVO_4$ as a photocatalyst on itself is experiencing rapid recombination of photogenerated charge carriers and inefficient charge transport properties [47,48]. Hence, the formation of heterojunction structure between 1D-ZnO nanorods and $BiVO_4$ nanocrystals is ideal to overcome the inherent drawbacks of these semiconductor materials while at the same time taking merits of the unidirectional electronic transmission channel in 1D-ZnO nanorods and robust light absorption properties in $BiVO_4$ nanocrystals.

Balachandran et al. reported the coupling of nanobundle-shaped $BiVO_4$/ZnO heterostructure synthesized through hydrothermal reaction followed by thermal decomposition [49]. They found that the photoactivities of $BiVO_4$/ZnO heterostructures over the degradation of Acid Violet 7 (96% degradation in 75 min), Evens Blue (99% degradation in 90 min), and Reactive Red 120 (~100% degradation in 75 min) were higher when compared to pristine ZnO, $BiVO_4$, and TiO_2-P25 under natural sunlight. The significant enhancement in photoactivity of $BiVO_4$/ZnO is attributed to the increased light absorption into the visible spectrum and matching energy band gap positions for efficient separation of photogenerated charge carriers. Yang and Wu fabricated Co-Pi/$BiVO_4$/ZnO heterojunction nanodendrite arrays on FTO substrate for PEC water oxidation [42]. They demonstrated that the heterojunction nanodendrite photoanode was fully-depleted at 0.8 V vs RHE by the electric fields, and this could facilitate the separation of the photogenerated charge carriers. The water oxidation reaction was improved when the photogenerated holes were drifted to the photoanode/electrolyte interface due to the radial motion of electric fields in the 1D-ZnO nanodendrite. More recently, Srinivasan and co-workers synthesized C-ZnO/$BiVO_4$ heterostructured nanocomposite from the coupling of $BiVO_4$ with carbon-doped ZnO nanoparticles via the hydrothermal reaction followed by mixing-ultrasonication process [50]. They found that the formation of C-ZnO/$BiVO_4$ nanocomposite is not only shifted the light absorption of ZnO towards the visible region, but also reduced the charge carriers recombination rate as well as increased the charge separation efficiency. Photocatalytic results showed that the C-ZnO/$BiVO_4$ nanocomposite degraded over 95% of MB dye within 50 min, which was faster than ZnO, C-ZnO, and $BiVO_4$ that required 120, 70, and 60 min, respectively, to attain a similar level of degradation rate of more than 95%.

Previous studies have demonstrated that the coupling of ZnO and $BiVO_4$ semiconductors typically resulted in a Type I band alignment heterojunction, whereby both photo-excited electrons and holes would migrate from ZnO to $BiVO_4$ due to the positions of their band edge potentials [49,51]. This has caused the accumulation of electrons and holes on a single semiconductor (ZnO) within the heterojunction structure, leading to negligible or little enhancement on the photocatalytic performance. To the best of our knowledge, this is the first and pioneering study reported on the successful fabrication of a novel heterojunction photocatalyst (in particulate system) with Type II band alignment between 1D-ZnO nanorods and $BiVO_4$ nanocrystals. Herein, pristine 1D-ZnO nanorods and $BiVO_4$ nanocrystals were first fabricated through the hydrothermal reaction followed by heterojunction formation via the wet chemical reaction. The resultant 1D-ZnO/$BiVO_4$ heterojunction photocatalysts were characterised using transmission electron microscopy (TEM), high resolution TEM (HRTEM), field emission-scanning electron microscopy (FE-SEM), energy dispersive X-ray (EDX) spectroscopy, X-ray diffraction (XRD), X-ray photoelectron spectroscopy (XPS), electrochemical impedance spectroscopy (EIS), photoluminescence (PL), and UV–visible (UV–vis) spectrophotometer. This was followed by water depollution experiments equipped with visible-light irradiation using the 1D-ZnO/$BiVO_4$ heterojunction photocatalysts in synthetic water containing both organic micropollutant and dye pollutant of salicylic acid (SA) and reactive black 5 (RB5), respectively. Finally, the outcomes from characterisation studies were referred to construct a theoretical heterojunction band alignment diagram constituting of 1D-ZnO nanorods and $BiVO_4$ nanocrystals as well as portraying the fundamental charge carriers (e^- and h^+) transfer within the 1D-ZnO/$BiVO_4$.

Experimental

Materials

Zinc acetate dihydrate ($Zn(CH_3COO)_2{\cdot}2H_2O$, 99%) was procured from HmBG Chemicals, Germany. Bismuth nitrate pentahydrate ($Bi(NO_3)_3{\cdot}5H_2O$) was obtained from R&M Chemicals, United Kingdom. Ammonium metavanadate (NH_4VO_3, 99%), methanol (CH_3OH, ≥99.9%), ethanol (C_2H_5OH, ≥99.9%), nitric acid (HNO_3, 69%), potassium hydroxide (KOH, 99%), and sodium sulphate (Na_2SO_4, ≥99%) were purchased from Merck, Germany. Sodium bicarbonate ($NaHCO_3$) was obtained from Thermo Fisher Scientific, United States. Commercial salicylic acid ($C_7H_6O_3$, 99%) and reactive black 5 (dye content 55%) were purchased from Sigma-Aldrich, Australia. All the purchased chemicals and reagents were of analytical grade and used as obtained without purification. Deionised water (>18.2 MΩ-cm resistivity) was used throughout the experiments to prepare aqueous solution.

Synthesis of 1D-ZnO nanorods

1D-ZnO nanorods were synthesized through a facile hydrothermal reaction using zinc acetate as the precursor. The synthesis method was adapted from our previous study [28]. Specifically, 29.5 g of $Zn(CH_3COO)_2{\cdot}2H_2O$ was dissolved in 125 mL methanol at 60 °C with continual stirring. Thereafter, a separate beaker containing 14.8 g of KOH dissolved with 65 mL methanol solution was slowly added into the previous Zn salt-containing mixture. The suspension was heated at 60 °C for 2 h in order to increase the Zn concentration in the solution. Following that, the concentrated Zn-containing solution was transferred into a 100 mL stainless-steel autoclave reactor. The hydrothermal reaction was maintained at 120 °C for 12 h before cooling to room temperature. Finally, the white powders were recovered by centrifugation and cleaned by washing with deionised water and ethanol alternatively for few times. The 1D-ZnO samples were then dried in an oven at 60 °C overnight.

Please cite this article in press as: J.S. Chang, et al., Exploration of a novel Type II 1D-ZnO nanorods/$BiVO_4$ heterojunction photocatalyst for water depollution, J. Ind. Eng. Chem. (2019), https://doi.org/10.1016/j.jiec.2019.12.002

Synthesis of $BiVO_4$ nanocrystals

Briefly, about 0.34 g of $Bi(NO_3)_3{\cdot}5H_2O$ was dissolved in 7 mL of 0.1 M nitric acid followed by filling up to a total volume of 35 mL with water. Meanwhile, 0.16 g of NH_4VO_3 was dissolved in 35 mL water. The Bi-HNO_3 solution and NH_4VO_3 solution were mixed together and stirred for 30 min to form a homogeneous solution. Following that, the pH of resulting solution was adjusted to neutral using $NaHCO_3$ and then transferred to the stainless-steel autoclave reactor in order to carry out the hydrothermal reaction at 100 °C for 6 h. After the reaction, the product was recovered through centrifugation and washed several times using deionised water and ethanol. Finally, the dried $BiVO_4$ sample was allowed to anneal at 400 °C for 1 h.

Synthesis of 1D-ZnO/$BiVO_4$ heterojunction photocatalysts

The 1D-ZnO/$BiVO_4$ heterojunction photocatalysts were prepared via a simple wet chemical reaction. Specifically, 0.1 g of 1D-ZnO nanorods was mixed in a solution consisting of 5 mL absolute ethanol and 5 mL water followed by 10 min of ultrasonication and 10 min of continuous stirring. Similarly, a varying weight amount of $BiVO_4$ nanocrystals was dispersed in a solution containing 5 mL absolute ethanol and 5 mL water followed by 10 min of ultrasonication and 10 min of continuous stirring. Subsequently, the $BiVO_4$ nanocrystals solution was added into the 1D-ZnO nanorods-containing solution gradually and stirred continuously for 1 h. Thereafter, the resulting 1D-ZnO/$BiVO_4$ solution was dried in an oven at 60 °C overnight. In this work, the weight amount of $BiVO_4$ was varied and the as-synthesized heterojunction photocatalysts were denoted as 1D-ZnO/$x$$BiVO_4$ (x = 0.02, 0.04, 0.06, 0.08, and 0.10 g, respectively).

Characterisation of photocatalysts

The physical structures and surface morphologies of pristine 1D-ZnO nanorods and $BiVO_4$ nanocrystals as well as the 1D-ZnO/$BiVO_4$ heterojunction photocatalysts were observed using a Hitachi SU8010 FE-SEM at an accelerating voltage of 5 kV, equipped with an EDX. Whilst the TEM and HRTEM which were used to observe the inner structures of the samples, were acquired using a JEOL JEM-2100F TEM operated at 200 kV. The degree of crystallinity of the as-synthesized photocatalysts were characterised using an XRD (Bruker D8 Discover) employed with Ni-filtered Cu-Kα radiation (λ = 0.1549 nm). The XRD scan was run with 40 kV and 40 mA at 0.02° s^{-1} scan rate. XPS measurements were carried out by using a scanning X-ray microprobe ULVAC-PHI Quantera II. The X-ray source of monochromatic Al-Kα (hv = 1486.6 eV) was applied at 15 kV with an output power of 25 W. Prior to the deconvolution of peaks, all binding energies were calibrated to the adventitious carbon signal (C 1s peak) at 284.6 eV [52]. The PL emission spectra were characterised in the wavelength range of 350–800 nm using a fluorescence spectrophotometer (Perkin Elmer LS55) with an excitation wavelength fixed at 325 nm. Diffuse reflectance spectra (DRS) of the photocatalysts were obtained using a UV–vis spectrophotometer (Agilent Cary 100) equipped with an integrating sphere for uniform scattering or diffusing effect. Barium sulphate was employed as the reference standard for DRS measurement. The UV–vis absorbance spectra of the as-synthesized photocatalysts were analysed within the wavelength range of 200–800 nm under ambient temperature.

Electrochemical analysis

The electrochemical characterisations of the 1D-ZnO/$BiVO_4$ heterojunction photocatalysts were carried out using an Autolab potentiostat unit (Metrohm PGSTAT 204 model, Netherlands). The potentiostat unit was setup based on a conventional three-electrode chemical cell, which consists of a working electrode (i.e. 1D-ZnO/$BiVO_4$ deposited on FTO), a counter electrode (i.e. platinum rod), and a reference electrode (i.e. Ag/AgCl saturated in 3 M KCl). The working electrode was prepared by dispersing the as-synthesized 1D-ZnO/$BiVO_4$ samples in isopropyl alcohol suspension with the concentration of 5 mg/mL followed by drop-casting onto the FTO glass substrate. A 150 W Xenon light with an illumination intensity of 100 mW/cm^2 was used as the visible-light irradiation source for the photocatalytic reaction. All the Nyquist impedance, transient photocurrent, and Mott–Schottky measurements were carried out using a 0.5 M Na_2SO_4 (pH 7 ± 0.2) electrolyte. Electrochemical impedance spectra (EIS) were conducted with a frequency range of 100 kHz – 0.1 Hz and at an amplitude of −0.5 V. Next, the transient photocurrent responses of the samples were examined at 0.2 V bias voltage for a duration of 5 min with 10 cycles of on and off visible-light irradiation. Mott–Schottky analyses were performed at frequency of 10 kHz within the potential scanning range of -2.0 – 0.2 V at a 0.05 V s^{-1} sweep rate.

Water depollution experiments

Photoactivities of the as-prepared photocatalysts were experimented for water depollution containing model organic micropollutant of SA and organic dye pollutant of RB5 in aqueous solution under visible-light irradiation. The photocatalytic reactor system was equipped with a 15 W cool daylight twist-shape bulb (Philips, TORNADO 15 W E27 220–240 V 50–60 Hz), which was placed on top of the photocatalytic beaker with a distance of 8 cm apart. The average intensity of the irradiated visible-light on the reacting medium was 8.5 mW cm^{-2}, which was measured using a pyranometer (Kipp and Zonen type CMP 6). In a typical water depollution experiment, 50 mg of the photocatalyst (i.e. ZnO, $BiVO_4$, and 1D-ZnO/$BiVO_4$ heterojunction photocatalysts) was dispersed into 50 mL of 10 ppm model organic SA or RB5 dye aqueous solution under constant magnetic stirring and ambient condition. Prior to the visible-light irradiation, the suspension was stirred in the dark for 30 min in order to achieve adsorption-desorption equilibrium between the model pollutant and photocatalysts. At every 20-min of time interval, 1.5 mL of the suspension was sampled from photocatalytic medium and centrifuged in order to completely separate the solid photocatalysts from the aqueous solution. The centrifuged clear solution was measured for their corresponding characteristic absorption peaks (i.e. λ_{max} = 297 nm for SA; λ_{max} = 597 nm for RB5) using a UV–vis spectrophotometer. The variation in absorbance values of SA and RB5 was recorded in order to examine the photodegradation efficiency according to the following equation:

$$\text{Photodegradation efficiency}(\%) = \frac{C_O - C_t}{C_t} \times 100\% \quad (1)$$

where C_O is the initial absorbance value of SA or RB5 after 30 min adsorption-desorption equilibrium in dark, and C_t is the absorbance value of SA or RB5 at specific irradiation time (t).

Besides, the cyclic stability and reusability of the 1D-ZnO/0.08$BiVO_4$ heterojunction photocatalyst were tested. After every round of photocatalysis, the samples were collected by centrifugation and washed with deionised water and ethanol for few times. After drying at 60 °C overnight, the 1D-ZnO/0.08$BiVO_4$ heterojunction photocatalyst was reused for a new batch of reaction with fresh SA or RB5 aqueous solution under the identical reaction conditions.

Please cite this article in press as: J.S. Chang, et al., Exploration of a novel Type II 1D-ZnO nanorods/$BiVO_4$ heterojunction photocatalyst for water depollution, J. Ind. Eng. Chem. (2019), https://doi.org/10.1016/j.jiec.2019.12.002

Results and discussion

Phase crystallinity and structural characterisation

The phase purity and crystal structure of pristine 1D-ZnO nanorods, $BiVO_4$ nanocrystals, and 1D-ZnO/$BiVO_4$ heterojunction photocatalysts were characterised by using XRD as shown in Fig. 1. The distinct and intense peaks analysed from XRD spectra indicated all the as-synthesized photocatalyst samples were highly crystalline. The diffraction peaks of pristine 1D-ZnO nanorods at 31.5°, 34.2°, 36.0°, 47.3°, 56.4°, 62.6°, 67.7°, and 68.8° correspond to the (100), (002), (101), (102), (110), (103), (112), and (201) crystal planes, respectively. All these characteristic diffraction peaks of 1D-ZnO nanorods were found to be consistent with the crystalline planes of hexagonal wurtzite ZnO according to JCPDS card no. 36-1451 (a = 3.249 Å, c = 5.207 Å) [53,54]. Whilst the 2θ values observed at 18.5°, 18.9°, 28.6°, 30.4°, 39.7°, 42.1°, and 53.5° in the XRD spectra of $BiVO_4$ nanocrystals were well-indexed to the (110), (011), (121), (040), (211), (150), and (161) crystalline planes, respectively. These characteristic diffraction peaks of $BiVO_4$ nanocrystals were assigned to the crystal lattice planes of monoclinic scheelite $BiVO_4$ (JCPDS card no. 14-0688, space group $I2/a$, a = 5.195 Å, b =11.701 Å, c = 5.092 Å, β = 90.38°). After the formation of 1D-ZnO/$BiVO_4$ heterojunction photocatalysts, it can be observed that the introduction of $BiVO_4$ nanocrystals in 1D-ZnO nanorods does not alter their crystal phase or induce apparent shift in the characteristics peaks. The detection of overlapping characteristic diffraction peaks of 1D-ZnO nanorods and $BiVO_4$ nanocrystals in the heterojunction photocatalysts indicates that the latter has a two-phase composition, which are of hexagonal wurtzite ZnO and monoclinic scheelite $BiVO_4$. No other impurity diffraction peaks are observed in the XRD spectra.

Both the physical structure and surface morphology of the photocatalyst samples were further analysed using FE-SEM, TEM, and HRTEM imaging. Fig. 2a illustrates the successful formation of abundant rod-like 1D-ZnO nanostructures with varying length of 300–500 nm. All the 1D-ZnO nanorods possess smooth surfaces and spread randomly on the surface planes. TEM image (Fig. 2b) shows that the 1D-ZnO nanorods are typically 20–40 nm in diameter with well-rounded surfaces at both ends. Fig. 2c shows the lattice fringe spacing of 0.26 nm (inset) for 1D-ZnO nanorods is well-corresponded to the average facet spacing between two (0001) planes of hexagonal wurtzite ZnO [55,56]. This suggests that the 1D-ZnO nanorods have a preferred growth orientation along the [0001] of c-axis direction. Whilst the $BiVO_4$ nanocrystals are comprised of several stacking layered structures with irregular profiles as depicted in Fig. 2d. From Fig. 2e, it can be seen that the morphological formation of $BiVO_4$ nanocrystals as a flat planar with smooth surfaces. The smallest surfaces of $BiVO_4$ nanocrystals that can be attained were about 10 nm in diameter, while the largest diameters of the planar surfaces were in the range of 200 nm to a few micrometres. Fig. 2f (inset) delineates the HRTEM image measured at one area of the representative $BiVO_4$ nanocrystals and the interplanar spacing was found to be 0.31 nm corresponding to the (121) plane of the monoclinic scheelite $BiVO_4$ [29]. This was further confirmed by the measured XRD spectra, which showed that $BiVO_4$ nanocrystals have the intense (121) peak. Both FE-SEM (Fig. 2g) and TEM (Fig. 2h) images of 1D-ZnO/$BiVO_4$ heterojunction photocatalysts revealed the presence of both 1D-ZnO nanorods and $BiVO_4$ nanocrystals in the heterostructure formation. These images show that there are no significant morphological changes induced during the process of heterostructure formation. The $BiVO_4$ nanocrystals have a larger surface area than the 1D-ZnO nanorods, whereby the 1D-ZnO nanorods were dispersed on the surfaces of $BiVO_4$ nanocrystals.

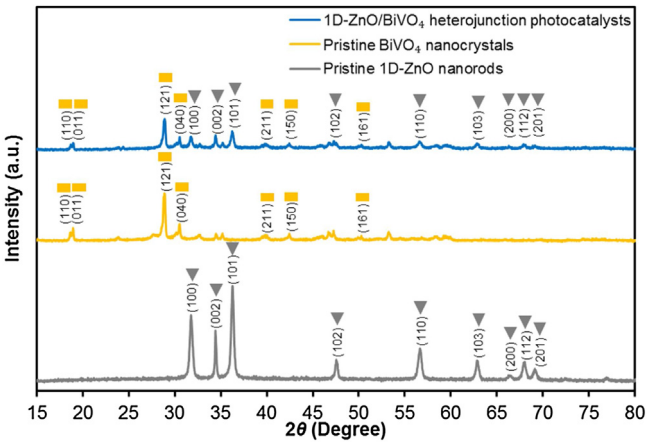

Fig. 1. XRD spectra of pristine 1D-ZnO nanorods, $BiVO_4$ nanocrystals, and 1D-ZnO/$BiVO_4$ heterojunction photocatalysts.

HRTEM images as delineated in Fig. 2i show the successful formation of 1D-ZnO/$BiVO_4$ heterojunction photocatalysts and the inner crystal structure consists of two sets of lattice spacings originated form ZnO and $BiVO_4$. One set (upper left inset Fig. 2i) of the measured fringe spacing of 0.31 nm was found to correspond to the (121) plane of the monoclinic scheelite crystal structure of $BiVO_4$. Whilst the second set (lower left inset Fig. 2i) of the measured fringe spacing of 0.26 nm was assigned to the (002) lattice spacing of the hexagonal wurtzite structure of ZnO. No distortion or separation of these 1D-ZnO/$BiVO_4$ heterojunction photocatalysts was observed even after ultrasonication for TEM sample preparation, which shows a strong bonding interaction between the 1D-ZnO nanorods and $BiVO_4$ nanocrystals. This is further verified in Fig. 2i showing the interlocked thin-crystal lattice fringes of the 1D-ZnO/$BiVO_4$ heterojunction photocatalysts instead of a simple physical overlapping of two individual nanostructures. This is favourable as the closely contacted interfaces between two different semiconductors allow for efficient charge transport and separation of charge carriers and therefore, enhancing the overall photoactivity [46,57].

The EDX analysis was performed on the 1D-ZnO/$BiVO_4$ heterojunction photocatalysts in order to determine the composition and distribution of chemical elements in the samples. According to the EDX spectra in Fig. 2j, 1D-ZnO/$BiVO_4$ heterojunction photocatalysts show the peaks for Zn, O, Bi, and V elements, signifying that there are no other impurity elements in the heterojunction photocatalysts. Additionally, the weight percentages of Zn, O, Bi, and V elements estimated from EDX analysis were found to be 16.22%, 21.12%, 51.43%, and 11.23%, respectively (inset table of Fig. 2j). The images of elemental mapping as shown in Fig. 2k–n illustrate that Zn, O, Bi, and V elements are well-defined spatially and homogeneously distributed in the maps. In accordance to the XRD results, the EDX analysis confirmed the successful formation of heterojunction between 1D-ZnO and $BiVO_4$ photocatalysts.

The surface composition and oxidation states of the chemical elements in 1D-ZnO/$BiVO_4$ heterojunction photocatalysts were further investigated by using XPS analysis. The XPS spectrum of as-synthesized 1D-ZnO/$BiVO_4$ revealed the presence of Zn, O, Bi, and V elemental characteristic peaks in the heterojunction structure (Fig. 3a). The high resolution XPS spectra of Zn 2p for 1D-ZnO/$BiVO_4$ heterojunction photocatalysts in Fig. 3b shows the binding energies of 1021.8 and 1044.9 eV corresponding to the signals Zn $2p_{3/2}$ and Zn $2p_{1/2}$, respectively [37]. It is concluded that Zn in the wurtzite ZnO with the +2 oxidation state is Zn^{2+}. O 1s XPS spectra (Fig. 3c) exhibit two deconvoluted peaks centred at 530.2 and 532.1 eV that could be ascribed to the presence of different kind of oxygen species. The peak position at 530.2 eV is mainly due

Please cite this article in press as: J.S. Chang, et al., Exploration of a novel Type II 1D-ZnO nanorods/$BiVO_4$ heterojunction photocatalyst for water depollution, J. Ind. Eng. Chem. (2019), https://doi.org/10.1016/j.jiec.2019.12.002

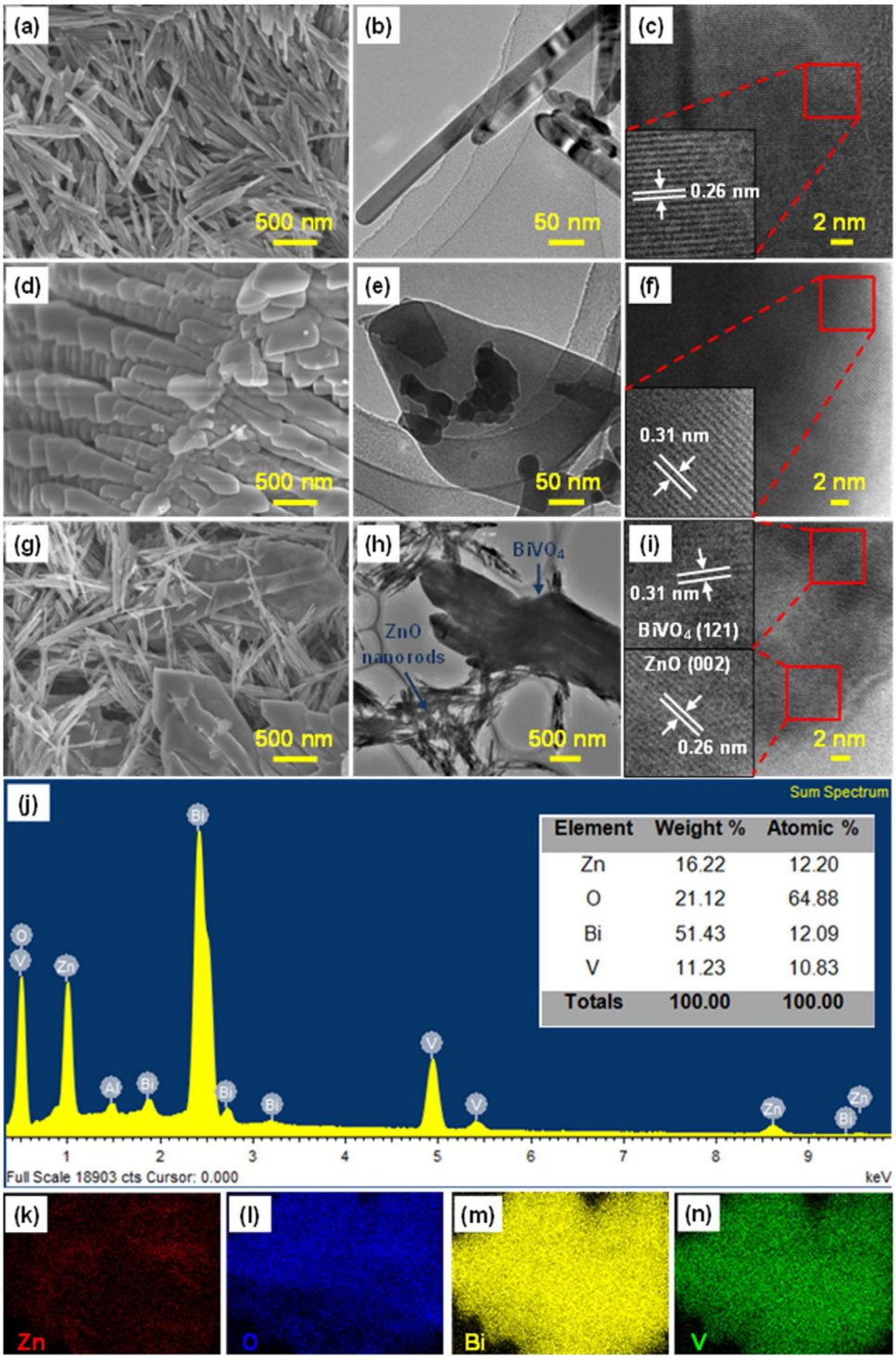

Fig. 2. FE-SEM images of (a) 1D-ZnO nanorods, (d) $BiVO_4$ nanocrystals, and (g) 1D-ZnO/$BiVO_4$ heterojunction photocatalysts. TEM images showing (b) 1D-ZnO nanorods, (e) $BiVO_4$ nanocrystals, and (h) 1D-ZnO/$BiVO_4$ heterojunction photocatalysts. HRTEM images of (c) 1D-ZnO nanorods, (f) $BiVO_4$ nanocrystals, and (i) 1D-ZnO/$BiVO_4$ heterojunction photocatalysts. (j) EDX spectra of 1D-ZnO/$BiVO_4$ heterojunction photocatalysts. Weight percentages of elements in 1D-ZnO/$BiVO_4$ heterojunction photocatalysts (inset table in Fig. 2j). (k–n) EDX elemental mapping images of 1D-ZnO/$BiVO_4$ heterojunction photocatalysts.

to the bonding of oxygen atoms with Zn atoms. Whilst the other noticeable peak at 532.1 eV is attributed to the OH group or water molecule adsorbed on the ZnO surface [57]. Furthermore, the peaks at binding energies of 158.2 (Bi $4f_{7/2}$) and 163.5 eV (Bi $4f_{5/2}$) as presented in Fig. 3d signify that bismuth is in the state of Bi^{3+} [58]. For the V 2p XPS spectra (Fig. 3e), the peaks located at 516.0 and 523.3 eV are assigned to V $2p_{3/2}$ and V $2p_{1/2}$, respectively [59]. The spin-orbital splitting of the components V $2p_{3/2}$ and V $2p_{1/2}$ also represents that vanadium in 1D-ZnO/$BiVO_4$ heterojunction photocatalysts is present as V^{5+}.

Furthermore, PL analysis as a direct indication on the charge transfer properties of semiconductors and also a qualitative measurement for recombination rate of photogenerated charge carriers was performed [60,61]. Fig. 4 depicts the comparison of PL

Please cite this article in press as: J.S. Chang, et al., Exploration of a novel Type II 1D-ZnO nanorods/$BiVO_4$ heterojunction photocatalyst for water depollution, J. Ind. Eng. Chem. (2019), https://doi.org/10.1016/j.jiec.2019.12.002

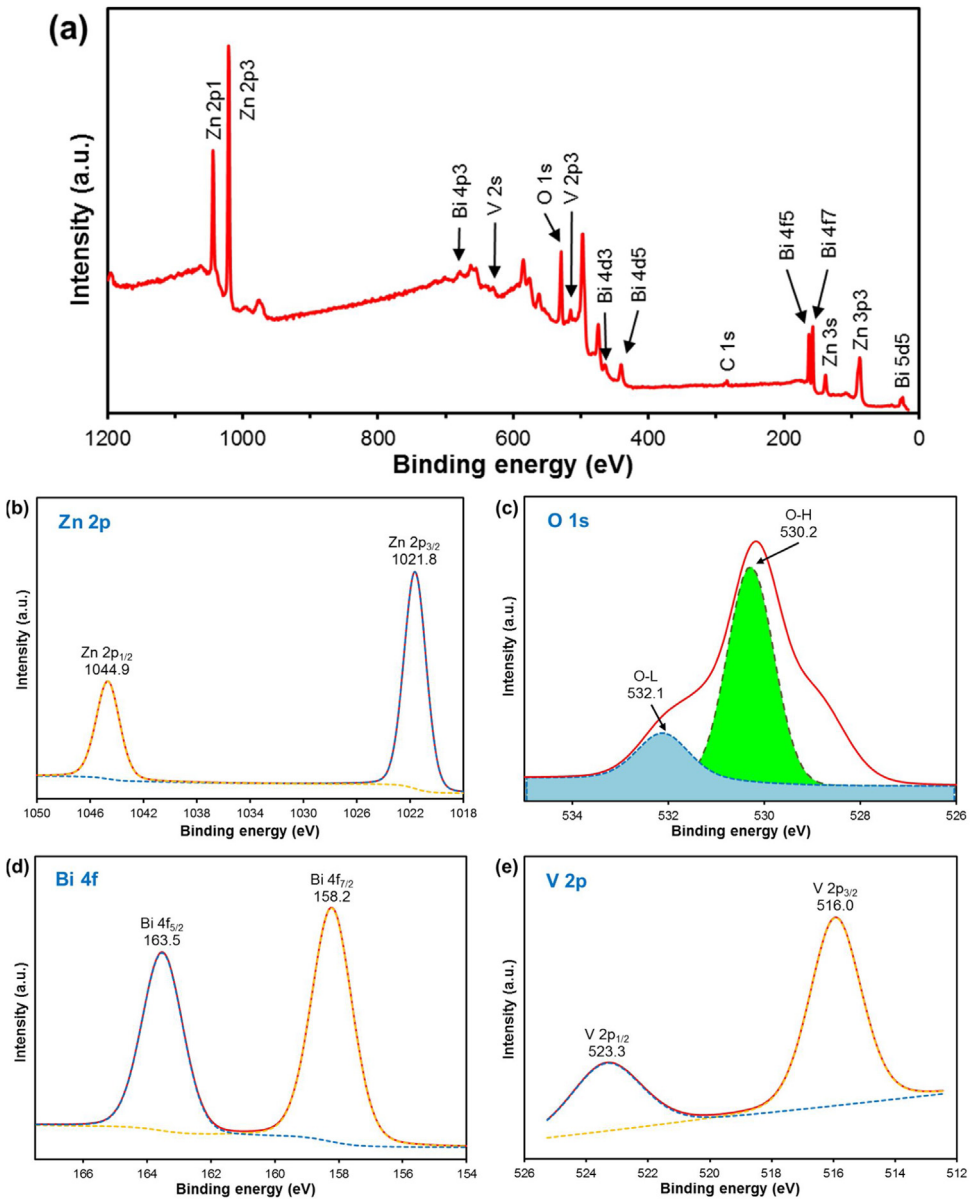

Fig. 3. (a) XPS survey spectrum, (b) Zn 2p, (c) O 1s, (d) Bi 4f, and (e) V 2p spectra of 1D-ZnO/$BiVO_4$ heterojunction photocatalysts.

emission spectra of pristine 1D-ZnO nanorods and $BiVO_4$ nanocrystals as well as 1D-ZnO/$BiVO_4$ heterojunction photocatalysts. The variation in PL intensity informs the recombination rate of photogenerated charge carriers among the samples [62,63]. As a matter of fact, sample with a higher charge recombination rate is characterised by a higher spectrum intensity during the PL analysis. From the PL emission spectra, it can be observed that the pristine ZnO exhibits an intense PL peak at 387.3 nm, which is equivalent to 3.30 eV corresponding to the near band edge emission. A broad and intense PL emission peak centered around 525 nm for $BiVO_4$ nanocrystals could be attributed to the recombination of intrinsic luminescence between valence band hole (i.e. hybrid orbitals of Bi 6s and O 2p) and conduction band electron (i.e. V 3d orbitals) [64]. It is evidenced that a reduction in the PL emission peak at 1D-ZnO characteristic wavelength of 387.3 nm for the heterojunction photocatalysts could be ascribed to the band gap narrowing resulted from the heterostructure formation with $BiVO_4$ nanocrystals. Moreover, the PL emission spectra validated that the 1D-ZnO/$BiVO_4$ heterojunction photocatalysts have a lower recombination rate of photogenerated charge carriers as the intensity of emission wavelength at 525 nm was lower than pristine $BiVO_4$ nanocrystals. From the analysis of different weight ratio of $BiVO_4$ in 1D-ZnO/x$BiVO_4$ in details, it is visible that the PL intensity peaks are arranged in the order of 1D-ZnO/0.08$BiVO_4$ < 1D-ZnO/0.10$BiVO_4$ < 1D-ZnO/0.06$BiVO_4$ < 1D-ZnO/0.04$BiVO_4$ < 1D-ZnO/0.02$BiVO_4$. The significantly lower intensity of the PL emission spectrum for the 1D-ZnO/0.08$BiVO_4$ implies a lower recombination rate of photogenerated charge carriers within the 1D-ZnO/0.08$BiVO_4$ implies a lower recombination rate of photogenerated charge carriers within the 1D-ZnO/0.08$BiVO_4$ heterojunction photocatalyst with a more efficient interfacial charge transfer and charge separation that could be beneficial for an improved photoactivity [65].

Electrochemical characterisations

EIS Nyquist analysis was used to determine the electrochemical behaviors, especially the interfacial charge transfer phenomenon and charge carriers separation efficiency in the heterojunction

Please cite this article in press as: J.S. Chang, et al., Exploration of a novel Type II 1D-ZnO nanorods/$BiVO_4$ heterojunction photocatalyst for water depollution, J. Ind. Eng. Chem. (2019), https://doi.org/10.1016/j.jiec.2019.12.002

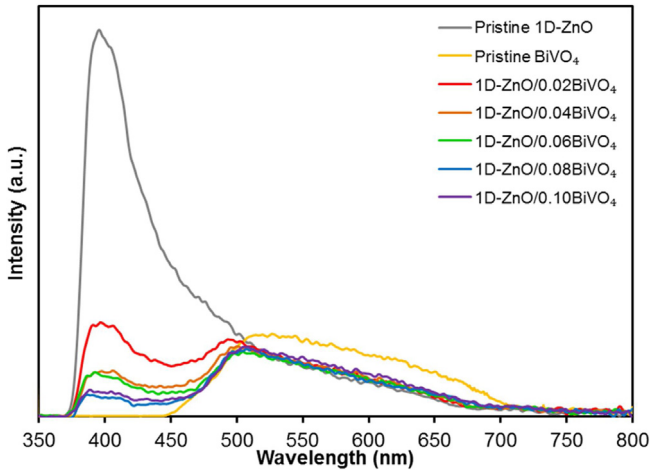

Fig. 4. PL emission spectra of pristine 1D-ZnO nanorods, $BiVO_4$ nanocrystals, and 1D-ZnO/$BiVO_4$ heterojunction photocatalysts.

photocatalysts [46,66]. Fig. 5 shows the Nyquist electrochemical impedance spectrum plots, where the *x*-axis represents the real part of impedance (Z′) while the *y*-axis denotes the imaginary part of impedance. Generally, the semicircular arc in the EIS Nyquist plot represents the charge transfer resistance (R_{ct}) at the heterostructure interface. In Fig. 5a, the smaller Nyquist arc radii imply a more rapid charge carriers transfer with a lower interfacial resistance for the 1D-ZnO/$BiVO_4$ heterojunction photocatalysts when compared to the pristine 1D-ZnO nanorods and $BiVO_4$ nanocrystals. This directly correlates to the photocatalytic performance, where the 1D-ZnO/$BiVO_4$ heterojunction photocatalysts exhibited a higher photoactivity than the pristine 1D-ZnO nanorods and $BiVO_4$ nanocrystals. As for the Nyquist plot showing the comparison of different weight ratio of $BiVO_4$ in 1D-ZnO/$BiVO_4$ heterojunction photocatalysts (Fig. 5b), it can be seen that the Nyquist arc radius is arranged in the descending order of 1D-ZnO/0.08$BiVO_4$ < 1D-ZnO/0.10$BiVO_4$ < 1D-ZnO/0.06$BiVO_4$ < 1D-ZnO/0.04$BiVO_4$ < 1D-ZnO/0.02$BiVO_4$. This is strongly correlated to the PL emission spectra analysis and agreed that the 1D-ZnO/0.08$BiVO_4$ heterojunction photocatalyst has the most rapid charge transfer with the lowest charge transfer resistance among other heterojunction photocatalysts, resulting in the highest photoactivity.

Furthermore, the charge transfer dynamics on the pristine 1D-ZnO nanorods, pristine $BiVO_4$ nanocrystals and 1D-ZnO/$BiVO_4$ heterojunction photocatalysts were further examined by transient photocurrent responses in Na_2SO_4 electrolyte at bias voltage of 0.2 V vs Ag/AgCl. Fig. 6 shows the chronoamperometric comparison of pristine 1D-ZnO nanorods and pristine $BiVO_4$ nanocrystals as well as the 1D-ZnO/$BiVO_4$ heterojunction photocatalysts under constant non-irradiated and visible-light irradiation conditions. It was observed that photocurrent density of pristine 1D-ZnO

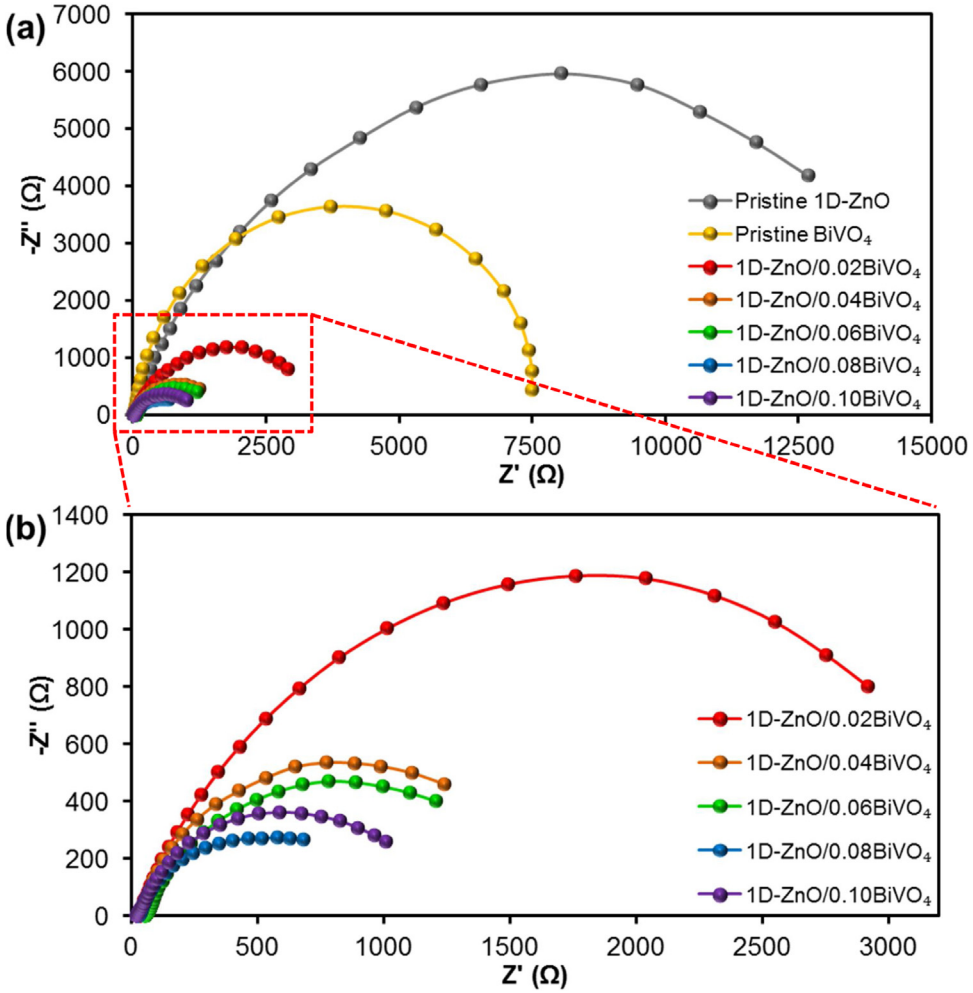

Fig. 5. EIS Nyquist plots for (a) pristine 1D-ZnO nanorods, pristine $BiVO_4$ nanocrystals and 1D-ZnO/$BiVO_4$ heterojunction photocatalysts and (b) magnified version for different weight ratio of $BiVO_4$ in 1D-ZnO/$BiVO_4$ heterojunction photocatalysts.

Please cite this article in press as: J.S. Chang, et al., Exploration of a novel Type II 1D-ZnO nanorods/$BiVO_4$ heterojunction photocatalyst for water depollution, J. Ind. Eng. Chem. (2019), https://doi.org/10.1016/j.jiec.2019.12.002

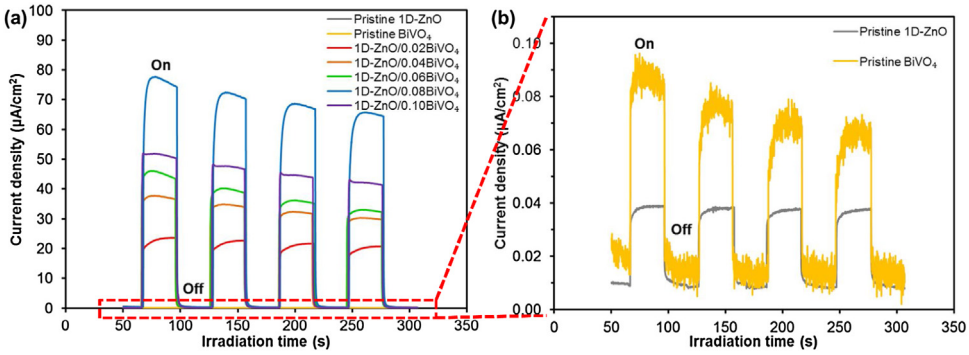

Fig. 6. Transient photocurrent responses of (a) pristine 1D-ZnO nanorods, pristine $BiVO_4$ nanocrystals and 1D-ZnO/$BiVO_4$ heterojunction photocatalysts and (b) enlarged plot for pristine 1D-ZnO nanorods and $BiVO_4$ nanocrystals measured at an applied potential of 0.2 V vs Ag/AgCl.

nanorods, pristine $BiVO_4$ nanocrystals and 1D-ZnO/$BiVO_4$ heterojunction photocatalysts increased significantly when the light irradiation was present, and dropped abruptly in non-irradiated condition. This transient behaviour is due to the relaxation effect during the photo-excitation and de-excitation processes [67]. The occurrence of photocurrent decay upon visible-light irradiation is associated with the rapid surface charge recombination rate due to the accumulation of photogenerated holes that hinders the effective charge transfer process at the interface between the 1D-ZnO/$BiVO_4$ heterojunction photocatalyst and electrolyte [68]. From Fig. 6a and b, it can be observed that the 1D-ZnO/$BiVO_4$ heterojunction photocatalysts possess significantly higher photocurrent density when compared to the pristine 1D-ZnO nanorods and $BiVO_4$ nanocrystals. The highest photocurrent density of 71.26 $\mu A/cm^2$ was achieved by 1D-ZnO/0.08$BiVO_4$, which was more than 1000-fold higher than pristine $BiVO_4$ of 0.07 $\mu A/cm^2$ and pristine ZnO of 0.04 $\mu A/cm^2$ upon visible-light irradiation. This again has proven that the 1D-ZnO/0.08$BiVO_4$ heterojunction photocatalyst was the best compositional weight ratio with high photoactivity that overcomes the inherent characteristic of rapid recombination rate encountered in pristine 1D-ZnO nanorods and $BiVO_4$ nanocrystals.

Water depollution and reusability experiments

The as-synthesized photocatalysts were applied for water depollution and the extent of their photoactivities were assessed by measuring the degradation rates of SA and RB5 under visible-light irradiation, as depicted in Fig. 7. The control experiments showed that organic micropollutant of SA and RB5 dye are resistant to self-photolysis with insignificant degradation rates (i.e. SA ~4% and RB5 ~5%). In the presence of pristine 1D-ZnO and $BiVO_4$ as photocatalysts, the photodegradation rates of SA and RB5 were in the range 7–24% (Fig. 7a) and 23–54% (Fig. 7c), respectively. A higher photoactivity in $BiVO_4$ nanocrystals is attributed to the narrower band gap energy of 2.4 eV, which allows light photon activation upon

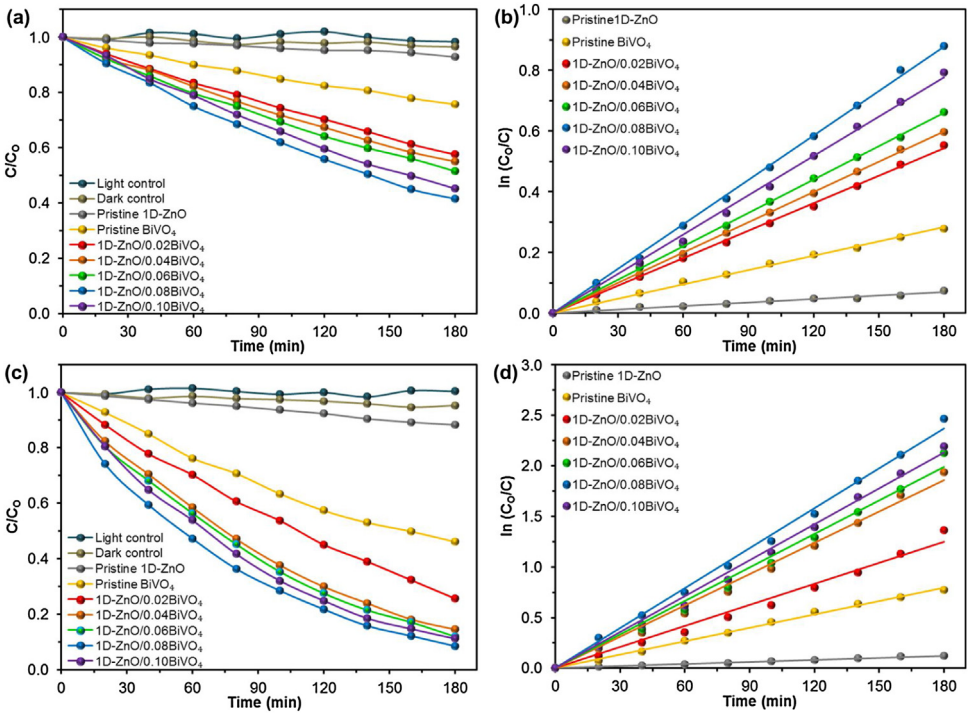

Fig. 7. Photodegradation of (a) SA and (c) RB5 over 1D-ZnO nanorods, $BiVO_4$ nanocrystals, and 1D-ZnO/$BiVO_4$ heterojunction photocatalysts under visible-light irradiation. Pseudo-first-order reaction rate constants for the photocatalytic degradation of (b) SA and (d) RB5 using 1D-ZnO nanorods, $BiVO_4$ nanocrystals, and 1D-ZnO/$BiVO_4$ heterojunction photocatalysts. Experimental parameters: photocatalyst loading of 50 mg; initial concentration of SA and RB5 of 10 ppm; natural pH; and temperature of 30 ± 1 °C.

Please cite this article in press as: J.S. Chang, et al., Exploration of a novel Type II 1D-ZnO nanorods/$BiVO_4$ heterojunction photocatalyst for water depollution, J. Ind. Eng. Chem. (2019), https://doi.org/10.1016/j.jiec.2019.12.002

visible-light irradiation. Additionally, simple physical dispersion of individual pristine 1D-ZnO and $BiVO_4$ in the photocatalytic media of SA and RB5 exhibited lower photodegradation efficiencies when compared to 1D-ZnO/$BiVO_4$ heterojunction photocatalyst (Fig. S1). This could be due to the minimal contact and weak bonding between the 1D-ZnO and $BiVO_4$ that reduces the effective charge carriers transfer within the photocatalysts. Among the synthesized samples, 1D-ZnO/0.08$BiVO_4$ heterojunction photocatalyst exhibited the highest visible-light photoactivity during the degradation of SA and RB5. Fig. 7a and c shows that the 1D-ZnO/0.08$BiVO_4$ heterojunction photocatalyst achieved the highest photodegradation efficiencies of 59% and 92% for SA and RB5, respectively upon 180 min of visible-light irradiation. It was found that the variation in weight ratio of $BiVO_4$ in the 1D-ZnO/$BiVO_4$ heterojunction photocatalysts resulted in an increasing photoactivity until the optimum weight ratio of 1:0.08 and dropped abruptly thereof. The presence of excessive $BiVO_4$ contents is known to cause light scattering phenomenon and occupy the active sites on the photocatalyst surface [69,70]. The improved visible-light photoactivity in the 1D-ZnO/0.08$BiVO_4$ photocatalyst is attributed to the low recombination rate of photogenerated charge carriers as a result of rapid charge transfer across interfaces between 1D-ZnO and $BiVO_4$ layers that associated with a low charge transfer resistance as evidenced from the PL and electrochemical studies.

As observed from Fig. 7b and d, the variation of model pollutant concentration in terms of $\ln(C_O/C)$ is directly proportional to the visible-light irradiation time. This validated that the photodegradation kinetics of SA and RB5 were well-fitted using the pseudo-first-order kinetics Langmuir-Hinshelwood rate equation of $\ln(C_O/C) = kt$, where C_O is the concentration of model pollutant after 30 min of adsorption-desorption equilibrium (ppm), C is the concentration at irradiation time t (ppm), and k is the pseudo-first-order reaction rate constant (min^{-1}). The calculated pseudo-first-order reaction rate constants k as indicated in Fig. 7b and d was found to be concordant to the photodegradation results as presented in Fig. 7a and c. The optimum 1D-ZnO/0.08$BiVO_4$ heterojunction photocatalyst achieved the highest pseudo-first-order reaction rate constants of 0.0049 min^{-1} and 0.0132 min^{-1} for SA and RB5 at a very high Pearson correlation value of $R^2 > 0.99$, respectively.

In addition, the stability and reusability of the 1D-ZnO/$BiVO_4$ heterojunction photocatalyst are of important concerns when being applied for practical water depollution. Thus, the reusability of the optimum 1D-ZnO/0.08$BiVO_4$ heterojunction photocatalyst was investigated over five identical reaction cycles for the degradation of SA and RB5. Fig. 8a and b shows that the optimum 1D-ZnO/0.08$BiVO_4$ heterojunction photocatalyst was highly stable and enabled reusability for practical water remediation as it demonstrated less than 10% loss of initial photodegradation efficiency after 5 reaction cycles, which is equivalent to a total reaction duration of 900 min. Moreover, FE-SEM imaging and EDX analysis were employed to evaluate the surface stability of heterojunction photocatalyst after photodegradation experiments. As shown in Fig. S2a and S2b, there is no apparent morphological change or structural alteration as can be observed. EDX spectra (Fig. S2c) confirmed that the 1D-ZnO/0.08$BiVO_4$ heterojunction photocatalyst is solely constituted of Zn, O, Bi, and V elements. The EDX mapping images in Fig. S2d–g reveal that the Zn, O, Bi, and V elements are uniformly dispersed within the selected screening areas. This study demonstrated that the optimum 1D-ZnO/0.08$BiVO_4$ heterojunction photocatalyst has a good catalytic stability by retaining high reactivity after five consecutive photodegradation cycles.

Photogenerated holes and free radicals trapping experiments

In order to investigate the possible photocatalytic mechanism and the specific roles of reactive oxygen species (ROS) on the degradation of SA and RB5 using 1D-ZnO/0.08$BiVO_4$ heterojunction photocatalyst, trapping experiments for ROS were conducted. In this study, isopropanol (IPA), triethanolamine (TEA), and p-benzoquinone (p-BQ) were used as quenchers to scavenge the ROS generated during the photocatalytic reaction using 1D-ZnO/0.08$BiVO_4$ heterojunction photocatalyst [71,72]. Specifically, the scavenging reagents of IPA, TEA, and p-BQ with the concentration of 10 mM in the photocatalytic reaction system were used to capture the active species of $^{\bullet}OH$, h^+, and $^{\bullet}O_2^-$, respectively. As observed from Fig. 9, the photodegradation rates for both SA and RB5 were significantly suppressed due to the quenching effect. The addition of IPA and TEA quenchers has a lower impact on the photodegradation efficiency of SA as compared to p-BQ quencher which reduced the SA degradation efficiency from 58.5% to 7.9% (Fig. 9a). Similar to the ROS trapping experiment for the photodegradation process of RB5 (Fig. 9b), the degradation rate of RB5 was remarkably hindered after adding with $^{\bullet}O_2^-$ scavenger (p-BQ), whereby the efficiency was dropped from 91.5% to 10.3%. In this instance, both the $^{\bullet}OH$ and photogenerated h^+ quenchers suppressed the photodegradation efficiency to a smaller extent when compared to the $^{\bullet}O_2^-$ quencher. This study indicates that $^{\bullet}O_2^-$ radicals are the dominant oxidative species of 1D-ZnO/0.08$BiVO_4$ for the photodegradation of SA and RB5; while $^{\bullet}OH$ radicals and photogenerated h^+ play an assistive role in the photocatalytic system.

Proposed photocatalytic mechanism for 1D-ZnO/$BiVO_4$ heterojunction photocatalyst

Prior to the construction of a theoretical band alignment diagram in explaining the plausible photocatalytic mechanism in the 1D-ZnO/$BiVO_4$ heterojunction photocatalyst, an in-depth analysis on its corresponding band gap energy and band gap position is vital. The experimental Mott–Schottky analysis was conducted to investigate the flat-band potential (E_{fb}) for pristine 1D-ZnO nanorods and $BiVO_4$ nanocrystals by measuring the space charge capacitance or junction capacitance of the semiconductors (C_{SC}) at different applied

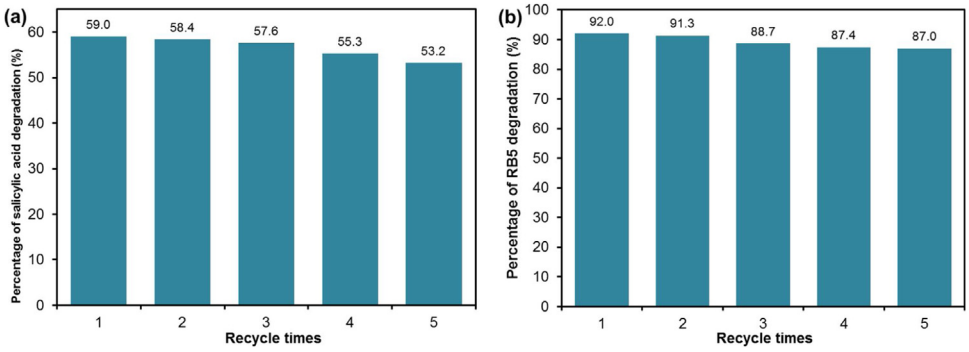

Fig. 8. Stability and reusability of 1D-ZnO/0.08$BiVO_4$ heterojunction photocatalyst for the degradation of (a) SA and (b) RB5.

Please cite this article in press as: J.S. Chang, et al., Exploration of a novel Type II 1D-ZnO nanorods/$BiVO_4$ heterojunction photocatalyst for water depollution, J. Ind. Eng. Chem. (2019), https://doi.org/10.1016/j.jiec.2019.12.002

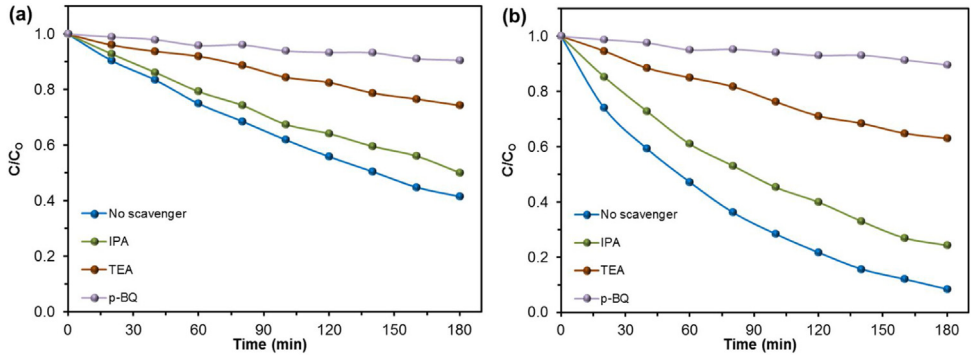

Fig. 9. The influence of different scavenging reagents on the photodegradation efficiency of (a) SA and (b) RB5 using 1D-ZnO/0.08$BiVO_4$ heterojunction photocatalysts under visible-light irradiation.

potentials (E). The E_{fb} of both the pristine photocatalysts can be estimated from the tangent straight line intercept to the x-axis in Mott–Schottky plots by using the following Eq. (1) [73]:

$$\frac{1}{C_{SC}^2} = \frac{2}{e\varepsilon\varepsilon_o N_d A_S^2}\left(E - E_{fb} - \frac{kT}{e}\right) \quad (2)$$

where C_{SC} is the semiconductor space charge layer capacitance (cm^3), e is the electronic charge (C), ε is the dielectric constant of semiconductor, ε_o is the permittivity of vacuum (F/cm), A_S is the surface area of working electrode (cm^2), E is the potential applied (V), k is the Boltzmann's constant, and T is the temperature (K). Based on Fig. 10a and b, it can be observed that both the pristine 1D-ZnO nanorods and $BiVO_4$ nanocrystals exhibited positive slopes in the Mott–Schottky plots, implying that both studied semiconductors are the n-type semiconductor. The estimated E_{fb} for pristine 1D-ZnO nanorods and $BiVO_4$ nanocrystals were −0.62 V and −1.48 V, respectively.

Additionally, the UV–vis spectroscopic measurements were conducted to characterise the optical properties and light absorption responses of pristine 1D-ZnO nanorods, pristine $BiVO_4$ nanocrystals and 1D-ZnO/$BiVO_4$ heterojunction photocatalysts, as exemplified in Fig. 10c. The pristine 1D-ZnO nanorods possessed the DRS curve pattern with an absorption band lower than 400 nm owing to the intense UV absorption [74]. Whilst the pristine $BiVO_4$ nanocrystals demonstrated a significant absorbance intensity at longer wavelength (~500 nm), which indicated that it is a visible-light active photocatalyst. It is also apparent that all the 1D-ZnO/$BiVO_4$ heterojunction photocatalysts exhibited both the optical properties of pristine 1D-ZnO nanorods and $BiVO_4$ nanocrystals. In this instance, the 1D-ZnO/$BiVO_4$ heterojunction photocatalysts showed a slightly weaker absorption band at 400 nm for ZnO and a strong light absorption characteristic at wavelength of 500 nm for $BiVO_4$. Thus, the formation of 1D-ZnO/$BiVO_4$ heterojunction photocatalysts was proven to induce a significant shift in its light

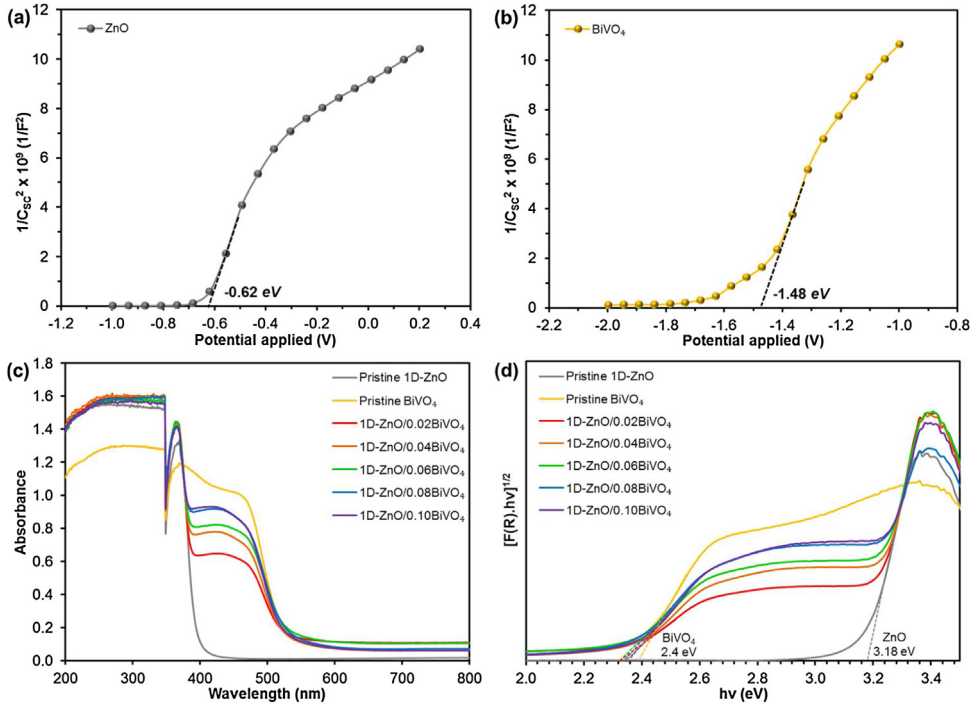

Fig. 10. Mott–Schottky analysis for pristine (a) 1D-ZnO nanorods and (b) $BiVO_4$ nanocrystals. (c) UV–vis diffuse reflectance spectra of pristine 1D-ZnO nanorods, $BiVO_4$ nanocrystals and 1D-ZnO/$BiVO_4$ heterojunction photocatalysts. (d) Tauc's plot for pristine 1D-ZnO nanorods, $BiVO_4$ nanocrystals and 1D-ZnO/$BiVO_4$ heterojunction photocatalysts.

Please cite this article in press as: J.S. Chang, et al., Exploration of a novel Type II 1D-ZnO nanorods/$BiVO_4$ heterojunction photocatalyst for water depollution, J. Ind. Eng. Chem. (2019), https://doi.org/10.1016/j.jiec.2019.12.002

absorption spectrum towards visible-light region with wavelength longer than 500 nm for improved photo-responsiveness.

Following this, the Tauc's plot was calculated from the UV–vis spectra to estimate the optical band gap energy (E_g) for pristine 1D-ZnO nanorods and $BiVO_4$ nanocrystals. The relationship between the absorption coefficient (α) and incident photon energy ($h\nu$) of semiconductor is as shown in the following equation:

$$\alpha h\nu = A(h\nu - E_g)^n \quad (3)$$

where A is a constant and n depends on the nature of transition and it was taken as $n = {}^1/_2$ for pristine 1D-ZnO nanorods and $BiVO_4$ nanocrystals [75]. Subsequently, the energy band gap values for the pristine 1D-ZnO nanorods, pristine $BiVO_4$ nanocrystals and 1D-ZnO/$BiVO_4$ heterojunction photocatalysts were estimated by extending the tangent lines of the curves to the interception of x-axis for Tauc's plot. Fig. 10d shows the extrapolated energy band gap values for pristine 1D-ZnO nanorods and pristine $BiVO_4$ nanocrystals are 3.18 eV and 2.40 eV, respectively. Interestingly, it was found that the optical energy band gap for the 1D-ZnO/$BiVO_4$ heterojunction photocatalysts was 2.32 eV which was lower than both the pristine 1D-ZnO nanorods and pristine $BiVO_4$ nanocrystals. The narrower energy band gap for the 1D-ZnO/$BiVO_4$ heterojunction photocatalysts also found to synergistically improve on its optical light absorption properties into the visible-light region in addition to the strong light absorption characteristic at wavelength longer than 500 nm as identified earlier.

Based on the Mott–Schottky analysis and Tauc's plots, a theoretical band alignment diagram was constructed for the 1D-ZnO/$BiVO_4$ heterojunction photocatalysts as shown in Fig. 11. This is crucial as the theoretical band diagram can be used to elucidate the photo-generated charge carriers transfer mechanism within 1D-ZnO/$BiVO_4$ heterojunction photocatalysts. Fig. 11 presents that the conduction band (CB) of pristine 1D-ZnO nanorods and $BiVO_4$ nanocrystals are measured at −0.62 eV and −1.48 eV, respectively. Whilst the valence band (VB) of pristine 1D-ZnO nanorods and $BiVO_4$ nanocrystals are located at +2.56 eV and +0.92 eV, respectively. Based on the fundamentals of hetero-junction formation, the 1D-ZnO/$BiVO_4$ heterojunction photocatalysts are identified of having the Type II heterojunction staggered arrange-ment [49]. Upon visible-light irradiation for the 1D-ZnO/$BiVO_4$ heterojunction photocatalysts, the photoexcited electrons from the CB of $BiVO_4$ will be transferred to the CB of 1D-ZnO due to the difference in electronegativity in order to achieve charge equilibrium and stabilisation within the heterostructure [76]. The accumulated electrons at the CB of 1D-ZnO are then travelled to the molecular oxygen species to form the reactive $^{\bullet}O_2^-$ radicals followed by the formation of oxidative $^{\bullet}OH$ radicals, which are indispensable for the photodegradation of SA and RB5. Meanwhile, the photogenerated holes at the VB of 1D-ZnO will migrate to the VB of $BiVO_4$ and further react with water molecules in aqueous solution to produce $^{\bullet}OH$ radicals for further photodegradation of SA and RB5. As a result, the high concentration of accumulated electrons near the CB of 1D-ZnO and accumulated holes at the VB of $BiVO_4$ lead to an ideal band edge reconstruction that could facilitate the effective charge carriers' separation and lower recombination rate as proven in the characterisation studies [77].

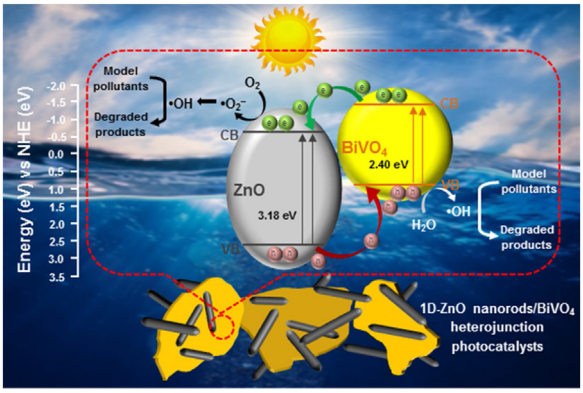

Fig. 11. Theoretical band diagram of 1D-ZnO/$BiVO_4$ heterojunction photocatalyst showing the plausible charge transfer and photocatalytic mechanisms for the degradation of SA and RB5 under visible-light irradiation.

Conclusion

In conclusion, a Type II 1D-ZnO/$BiVO_4$ heterojunction photo-catalyst (in particulate system) has been successfully synthesized for the first time via a facile combination of hydrothermal and wet-chemical reaction. The effects of varying $BiVO_4$ weight ratio in the 1D-ZnO/$BiVO_4$ heterojunction photocatalyst were systematically investigated for water depollution containing SA and RB5. The 1D-ZnO/$x$$BiVO_4$ heterojunction photocatalyst (x = weight ratio of $BiVO_4$ in g) that found optimum when x = 0.08 g exhibited high pseudo-first-order reaction rate constants of 0.0049 min^{-1} and 0.0132 min^{-1} for degradation of SA and RB5, respectively. Addition-ally, the optimum 1D-ZnO/0.08$BiVO_4$ heterojunction photocatalyst was found to be highly stable and enabled reusability for practical water remediation as it demonstrated less than 10% loss of its initial photodegradation efficiency after 5 reaction cycles, which is equivalent to a total reaction duration of 900 min. Moreover, the radicals trapping experiments confirmed that photogenerated h^+, $^{\bullet}O_2^-$, and $^{\bullet}OH$ played a decisive role in the photocatalytic system. The significant improvement in the photoactivity of 1D-ZnO/$BiVO_4$ heterojunction photocatalysts is attributed to the formation of a Type II heterojunction staggered arrangement that matches the band potentials and induces the synergistic effect of band edges between the 1D-ZnO nanorods and $BiVO_4$ nanocrystals. Besides, the optical and electrochemical studies also revealed that the enhanced photoactivity in 1D-ZnO/$BiVO_4$ heterojunction photocatalysts is ascribed to: (1) narrower energy band gap of 2.32 eV for low photon energy excitation (i.e. absorption into the visible-light spectrum of wavelength longer than 500 nm); (2) rapid charge transfer across interfaces between 1D-ZnO and $BiVO_4$ layers that comes with low charge transfer resistance; and (3) lower recombination rate and efficient separation of photogenerated charge carriers. This breakthrough study on developing a highly-efficient visible-light active 1D-ZnO/$BiVO_4$ heterojunction photo-catalyst with a favourable Type II staggered arrangement will open up a new vista in materials research and heterojunction engineering in advancing the practical water depollution application.

Declaration of interests

The authors declare that they have no known competing financial interests or personal relationships that could have appeared to influence the work reported in this paper.

Acknowledgements

The authors would like to thank Mr. Loo Hui Jie and Mr. Darren Low Yi Sern for their assistance in conducting the experiments. Prof. MN Chong is highly indebted to the Royal Society-Newton Advanced Fellowship (Reference No.: NA150418) awarded to him. Mr. Chang Jang Sen is thankful to the MyBrain15 scholarship from the Ministry of Higher Education, Malaysia.

Appendix A. Supplementary data

Supplementary material related to this article can be found, in the online version, at doi:https://doi.org/10.1016/j.jiec.2019.12.002.

References

[1] M.N. Chong, B. Jin, C.W.K. Chow, C. Saint, Water Res. 44 (2010) 2997, doi:http://dx.doi.org/10.1016/j.watres.2010.02.039.
[2] M.N. Chong, B. Jin, H.Y. Zhu, C.W.K. Chow, C. Saint, Chem. Eng. J. 150 (2009) 49, doi:http://dx.doi.org/10.1016/j.cej.2008.12.002.
[3] M.N. Chong, A.K. Sharma, S. Burn, C.P. Saint, J. Clean Prod. 35 (2012) 230, doi:http://dx.doi.org/10.1016/j.jclepro.2012.06.003.
[4] R. Andreozzi, V. Caprio, A. Insola, R. Marotta, Catal. Today 53 (1999) 51, doi:http://dx.doi.org/10.1016/S0920-5861(99)00102-9.
[5] Y. Xiang, J. Fang, C. Shang, Water Res. 90 (2016) 301, doi:http://dx.doi.org/10.1016/j.watres.2015.11.069.
[6] S. Garcia-Segura, J.D. Ocon, M.N. Chong, Process Saf. Environ. Prot. 113 (2018) 48, doi:http://dx.doi.org/10.1016/j.psep.2017.09.014.
[7] M.N. Chong, J. Sidhu, R. Aryal, J. Tang, W. Gernjak, B. Escher, S. Toze, Environ. Monit. Assess. 185 (2013) 6645, doi:http://dx.doi.org/10.1007/s10661-012-3053-7.
[8] M.N. Chong, A.N.M. Ho, T. Gardner, A.K. Sharma, B. Hood, J. Water Clim. Change 4 (2013) 338, doi:http://dx.doi.org/10.2166/wcc.2013.077.
[9] S. Dong, L. Xia, T. Guo, F. Zhang, L. Cui, X. Su, D. Wang, W. Guo, J. Sun, Appl. Surf. Sci. 445 (2018) 30, doi:http://dx.doi.org/10.1016/j.apsusc.2018.03.132.
[10] M.N. Chong, B. Jin, C.W.K. Chow, C.P. Saint, Chem. Eng. J. 152 (2009) 158, doi:http://dx.doi.org/10.1016/j.cej.2009.04.027.
[11] M.N. Chong, S. Lei, B. Jin, C. Saint, C.W.K. Chow, Sep. Purif. Technol. 67 (2009) 355, doi:http://dx.doi.org/10.1016/j.seppur.2009.04.001.
[12] Y. Nosaka, A.Y. Nosaka, Chem. Rev. 117 (2017) 11302, doi:http://dx.doi.org/10.1021/acs.chemrev.7b00161.
[13] J.S. Chang, J.K. Tan, S.N. Shah, A. Mateblowski, J. Strunk, P.E. Poh, M.N. Chong, J. Taiwan Inst. Chem. Eng. 81 (2017) 206, doi:http://dx.doi.org/10.1016/j.jtice.2017.10.030.
[14] L. Tan, C. Yu, M. Wang, S. Zhang, J. Sun, S. Dong, J. Sun, Appl. Surf. Sci. 467–468 (2019) 286, doi:http://dx.doi.org/10.1016/j.apsusc.2018.10.067.
[15] Z.L. Wang, J. Song, Science 312 (2006) 242, doi:http://dx.doi.org/10.1126/science.1124005.
[16] M. Pirhashemi, A. Habibi-Yangjeh, S. Rahim Pouran, J. Ind. Eng. Chem. 62 (2018) 1, doi:http://dx.doi.org/10.1016/j.jiec.2018.01.012.
[17] Y. Jin, J. Wang, B. Sun, J.C. Blakesley, N.C. Greenham, Nano Lett. 8 (2008) 1649, doi:http://dx.doi.org/10.1021/nl0803702.
[18] C.B. Ong, L.Y. Ng, A.W. Mohammad, Renew. Sustain. Energ. Rev. 81 (2018) 536, doi:http://dx.doi.org/10.1016/j.rser.2017.08.020.
[19] J.-J. Wu, S.-C. Liu, Adv. Mater. 14 (2002) 215, doi:http://dx.doi.org/10.1002/1521-4095(20020205)14:3<215::AID-ADMA215>3.0.CO;2-J.
[20] Y. Zhang, Y. Wu, H. Ding, Y. Yan, Z. Zhou, Y. Ding, N. Liu, Nano Energy 53 (2018) 666, doi:http://dx.doi.org/10.1016/j.nanoen.2018.09.021.
[21] L. Vayssieres, Adv. Mater. 15 (2003) 464, doi:http://dx.doi.org/10.1002/adma.200390108.
[22] S. Qiao, J. Liu, G. Fu, K. Ren, Z. Li, S. Wang, C. Pan, Nano Energy 49 (2018) 508, doi:http://dx.doi.org/10.1016/j.nanoen.2018.04.070.
[23] S.J. Chen, Y.C. Liu, C.L. Shao, R. Mu, Y.M. Lu, J.Y. Zhang, D.Z. Shen, X.W. Fan, Adv. Mater. 17 (2005) 586, doi:http://dx.doi.org/10.1002/adma.200401263.
[24] Z. Geng, X. Kong, W. Chen, H. Su, Y. Liu, F. Cai, G. Wang, J. Zeng, Angew. Chem. Int. Ed. 57 (2018) 6054, doi:http://dx.doi.org/10.1002/anie.201711255.
[25] B. Zhang, L. Lu, Q. Hu, F. Huang, Z. Lin, Biosens. Bioelectron. 56 (2014) 243, doi:http://dx.doi.org/10.1016/j.bios.2014.01.026.
[26] L. Zhu, Y. Li, W. Zeng, Appl. Surf. Sci. 427 (2018) 281, doi:http://dx.doi.org/10.1016/j.apsusc.2017.08.229.
[27] H. Kim, K. Yong, Phys. Chem. Chem. Phys. 15 (2013) 2109, doi:http://dx.doi.org/10.1039/C2CP44045H.
[28] J.S. Chang, J. Strunk, M.N. Chong, P.E. Poh, J.D. Ocon, J. Hazard. Mater. 381 (2020)120958, doi:http://dx.doi.org/10.1016/j.jhazmat.2019.120958.
[29] L. Yan, W. Zhao, Z. Liu, Dalton Trans. 45 (2016) 11346, doi:http://dx.doi.org/10.1039/C6DT02027E.
[30] X. Jiang, F.L. Wong, M.K. Fung, S.T. Lee, Appl. Phys. Lett. 83 (2003) 1875, doi:http://dx.doi.org/10.1063/1.1605805.
[31] S. Cho, J.-W. Jang, J.S. Lee, K.-H. Lee, CrystEngComm 12 (2010) 3929, doi:http://dx.doi.org/10.1039/C0CE00063A.
[32] P. Pascariu, I.V. Tudose, M. Suchea, E. Koudoumas, N. Fifere, A. Airinei, Appl. Surf. Sci. 448 (2018) 481, doi:http://dx.doi.org/10.1016/j.apsusc.2018.04.124.
[33] D.-T. Ngo, L.T. Cuong, N.H. Cuong, C.T. Son, P.T. Huy, N.D. Dung, Adv. Funct. Mater. 28 (2018)1704567, doi:http://dx.doi.org/10.1002/adfm.201704567.
[34] L. Jing, D. Wang, B. Wang, S. Li, B. Xin, H. Fu, J. Sun, J. Mol. Catal. A Chem. 244 (2006) 193, doi:http://dx.doi.org/10.1016/j.molcata.2005.09.020.
[35] C. de Melo, M. Jullien, Y. Battie, A. En Naciri, J. Ghanbaja, F. Montaigne, J.-F. Pierson, F. Rigoni, N. Almqvist, A. Vomiero, S. Migot, F. Mücklich, D. Horwat, ACS Appl. Mater. Interfaces 10 (2018) 40958, doi:http://dx.doi.org/10.1021/acsami.8b17194.
[36] W. Li, G. Wang, Y. Feng, Z. Li, Appl. Surf. Sci. 428 (2018) 154, doi:http://dx.doi.org/10.1016/j.apsusc.2017.09.049.
[37] A. Raja, P. Rajasekaran, K. Selvakumar, M. Arunpandian, K. Kaviyarasu, S. Asath Bahadur, M. Swaminathan, Sep. Purif. Technol. 233 (2020)115996, doi:http://dx.doi.org/10.1016/j.seppur.2019.115996.
[38] C. Wang, X. Wang, B.-Q. Xu, J. Zhao, B. Mai, P.A. Peng, G. Sheng, J. Fu, J. Photochem. Photobiol. A Chem. 168 (2004) 47, doi:http://dx.doi.org/10.1016/j.jphotochem.2004.05.014.
[39] H. Derikvandi, A. Nezamzadeh-Ejhieh, J. Hazard. Mater. 321 (2017) 629, doi:http://dx.doi.org/10.1016/j.jhazmat.2016.09.056.
[40] A. Shirzadi, A. Nezamzadeh-Ejhieh, J. Mol. Catal. A Chem. 411 (2016) 222, doi:http://dx.doi.org/10.1016/j.molcata.2015.10.027.
[41] J. Wang, Y. Xia, H. Zhao, G. Wang, L. Xiang, J. Xu, S. Komarneni, Appl. Catal. B Environ. 206 (2017) 406, doi:http://dx.doi.org/10.1016/j.apcatb.2017.01.067.
[42] J.-S. Yang, J.-J. Wu, Nano Energy 32 (2017) 232, doi:http://dx.doi.org/10.1016/j.nanoen.2016.12.039.
[43] Y.W. Phuan, W.-J. Ong, M.N. Chong, J.D. Ocon, J. Photochem. Photobiol. C Photochem. Rev. 33 (2017) 54, doi:http://dx.doi.org/10.1016/j.jphotochemrev.2017.10.001.
[44] Y. Park, K.J. McDonald, K.-S. Choi, Chem. Soc. Rev. 42 (2013) 2321, doi:http://dx.doi.org/10.1039/C2CS35260E.
[45] Z.-F. Huang, L. Pan, J.-J. Zou, X. Zhang, L. Wang, Nanoscale 6 (2014) 14044, doi:http://dx.doi.org/10.1039/C4NR05245E.
[46] C.S. Yaw, Q. Ruan, J. Tang, A.K. Soh, M.N. Chong, Chem. Eng. J. 364 (2019) 177, doi:http://dx.doi.org/10.1016/j.cej.2019.01.179.
[47] R. Crespo-Otero, A. Walsh, J. Phys. Chem. Lett. 6 (2015) 2379, doi:http://dx.doi.org/10.1021/acs.jpclett.5b00966.
[48] M. Arif, Z. Min, L. Yuting, H. Yin, X. Liu, J. Ind. Eng. Chem. 69 (2019) 345, doi:http://dx.doi.org/10.1016/j.jiec.2018.09.026.
[49] S. Balachandran, N. Prakash, K. Thirumalai, M. Muruganandham, M. Sillanpää, M. Swaminathan, Ind. Eng. Chem. Res. 53 (2014) 8346, doi:http://dx.doi.org/10.1021/ie404287m.
[50] N. Srinivasan, M. Anbuchezhiyan, S. Harish, S. Ponnusamy, Appl. Surf. Sci. 494 (2019) 771, doi:http://dx.doi.org/10.1016/j.apsusc.2019.07.093.
[51] X. She, Z. Zhang, M. Baek, K. Yong, Appl. Surf. Sci. 429 (2018) 29, doi:http://dx.doi.org/10.1016/j.apsusc.2017.06.257.
[52] J. Moudler, W. Stickle, P. Sobol, K. Bomben, Handbook of X-ray Photoelectron Spectroscopy, Perkin-Elmer Corp., Eden Praire, USA, 1992.
[53] M. Pirhashemi, A. Habibi-Yangjeh, Sep. Purif. Technol. 193 (2018) 69, doi:http://dx.doi.org/10.1016/j.seppur.2017.11.007.
[54] Y.-L. Hu, Z. Wu, X. Zheng, N. Lin, Y. Yang, J. Zuo, D. Sun, C. Jiang, L. Sun, C. Lin, Y. Fu, J. Alloys Compd. 709 (2017) 42, doi:http://dx.doi.org/10.1016/j.jallcom.2017.02.124.
[55] B. Cheng, E.T. Samulski, Chem. Commun. (2004) 986, doi:http://dx.doi.org/10.1039/B316435G.
[56] U. Pal, P. Santiago, J. Phys. Chem. B 109 (2005) 15317, doi:http://dx.doi.org/10.1021/jp052496i.
[57] S. Singh, R. Sharma, B.R. Mehta, Appl. Surf. Sci. 411 (2017) 321, doi:http://dx.doi.org/10.1016/j.apsusc.2017.03.189.
[58] X. Bai, M. Ji, M. Xu, N. Su, J. Zhang, J. Wang, C. Zhu, Y. Yao, B. Li, Inorg. Chem. Front. 6 (2019) 1097, doi:http://dx.doi.org/10.1039/C9QI00116F.
[59] J. Zhang, Y. Lu, L. Ge, C. Han, Y. Li, Y. Gao, S. Li, H. Xu, Appl. Catal. B Environ. 204 (2017) 385, doi:http://dx.doi.org/10.1016/j.apcatb.2016.11.057.
[60] S. Dong, X. Ding, T. Guo, X. Yue, X. Han, J. Sun, Chem. Eng. J. 316 (2017) 778, doi:http://dx.doi.org/10.1016/j.cej.2017.02.017.
[61] V. Shanmugam, S. Sanjeevamuthu, K.S. Jeyaperumal, R. Vairamuthu, J. Ind. Eng. Chem. 76 (2019) 318, doi:http://dx.doi.org/10.1016/j.jiec.2019.03.056.
[62] Y.W. Phuan, E. Ibrahim, M.N. Chong, T. Zhu, B.-K. Lee, J.D. Ocon, E.S. Chan, Appl. Surf. Sci. 392 (2017) 144, doi:http://dx.doi.org/10.1016/j.apsusc.2016.09.046.
[63] S. Dong, Y. Pi, Q. Li, L. Hu, Y. Li, X. Han, J. Wang, J. Sun, J. Alloys Compd. 663 (2016) 1, doi:http://dx.doi.org/10.1016/j.jallcom.2015.12.027.
[64] L. Shan, Y. Liu, J. Mol. Catal. A Chem. 416 (2016) 1, doi:http://dx.doi.org/10.1016/j.molcata.2016.02.013.
[65] H. Yi, M. Jiang, D. Huang, G. Zeng, C. Lai, L. Qin, C. Zhou, B. Li, X. Liu, M. Cheng, W. Xue, P. Xu, C. Zhang, J. Taiwan Inst. Chem. Eng. 93 (2018) 184, doi:http://dx.doi.org/10.1016/j.jtice.2018.06.037.
[66] S. Dong, L. Cui, C. Liu, F. Zhang, K. Li, L. Xia, X. Su, J. Feng, Y. Zhu, J. Sun, J. Taiwan Inst. Chem. Eng. 97 (2019) 288, doi:http://dx.doi.org/10.1016/j.jtice.2019.02.016.
[67] J. Tong, L. Zhang, F. Li, M. Li, S. Cao, Phys. Chem. Chem. Phys. 17 (2015) 23532, doi:http://dx.doi.org/10.1039/C5CP04057D.
[68] H. Yi, M. Yan, D. Huang, G. Zeng, C. Lai, M. Li, X. Huo, L. Qin, S. Liu, X. Liu, B. Li, H. Wang, M. Shen, Y. Fu, X. Guo, Appl. Catal. B Environ. 250 (2019) 52, doi:http://dx.doi.org/10.1016/j.apcatb.2019.03.008.
[69] X.-J. Lv, S.-X. Zhou, C. Zhang, H.-X. Chang, Y. Chen, W.-F. Fu, J. Mater. Chem. 22 (2012) 18542, doi:http://dx.doi.org/10.1039/C2JM33325B.
[70] M.N. Chong, Y.J. Cho, P.E. Poh, B. Jin, J. Clean Prod. 89 (2015) 196, doi:http://dx.doi.org/10.1016/j.jclepro.2014.11.014.
[71] S. Dong, L. Cui, Y. Zhao, Y. Wu, L. Xia, X. Su, C. Zhang, D. Wang, W. Guo, J. Sun, Appl. Surf. Sci. 463 (2019) 659, doi:http://dx.doi.org/10.1016/j.apsusc.2018.09.006.
[72] S. Dong, L. Xia, F. Zhang, F. Li, Y. Wang, L. Cui, J. Feng, J. Sun, J. Alloys Compd. 810 (2019)151955, doi:http://dx.doi.org/10.1016/j.jallcom.2019.151955.
[73] Y.W. Phuan, M.N. Chong, O. Satokhee, A.B. De Souza, T. Zhu, E.S. Chan, Part. Part. Syst. Charact. 34 (2017)1600216, doi:http://dx.doi.org/10.1002/ppsc.201600216.
[74] W.-H. Lam, M.N. Chong, B.A. Horri, B.-T. Tey, E.-S. Chan, J. Appl. Polym. Sci. 134 (2017), doi:http://dx.doi.org/10.1002/app.45002.
[75] Y. Liu, H. Dai, J. Deng, L. Zhang, C.T. Au, Nanoscale 4 (2012) 2317, doi:http://dx.doi.org/10.1039/C2NR12046A.
[76] W.-J. Ong, J.-J. Yeong, L.-L. Tan, B.T. Goh, S.-T. Yong, S.-P. Chai, RSC Adv. 4 (2014) 59676, doi:http://dx.doi.org/10.1039/C4RA10467F.
[77] D.-K. Ma, M.-L. Guan, S.-S. Liu, Y.-Q. Zhang, C.-W. Zhang, Y.-X. He, S.-M. Huang, Dalton Trans. 41 (2012) 5581, doi:http://dx.doi.org/10.1039/C2DT30099K.

Please cite this article in press as: J.S. Chang, et al., Exploration of a novel Type II 1D-ZnO nanorods/$BiVO_4$ heterojunction photocatalyst for water depollution, J. Ind. Eng. Chem. (2019), https://doi.org/10.1016/j.jiec.2019.12.002